A universal canopy gap fraction model for forests with various tree distributions based on Nilson's models considering directional overlaps among crowns

Jun Geng, Jean-Louis Roujean, Andres Kuusk, Yong Pang, Lili Tu, Teng Zhang, Jingsong Xu, Jing M Chen

A universal canopy gap fraction model for forests with various tree distributions based on Nilson's models considering directional overlaps among crowns

Jun Geng [a,b,1], Jean-Louis Roujean [b,1], Andres Kuusk [c,1], Yong Pang [d], Lili Tu [e,b,*], Teng Zhang [a], Jing M. Chen [f,g,*]

[a] *Hefei University of Technology, Hefei 230009, China*

[b] *Centre d'Etudes Spatiales de la BIOsphère (CESBIO), Toulouse III University, Toulouse 31400, France*

[c] *Tartu Observatory, University of Tartu, Tõravere 61602, Estonia*

[d] *Institute of Forest Resource Information Technique, Chinese Academy of Forestry, Beijing 100091, China*

[e] *College of Resources and Environment, Anhui Agricultural University, Hefei 23000, China*

[f] *School of Geographical Sciences, Fujian Normal University, Fuzhou 350108, China*

[g] *Department of Geography and Program in Planning, University of Toronto, Toronto, ON M5S 3G3, Canada*

[*] *Corresponding author. E-mail addresses: tulili@ahau.edu.cn (L. Tu); jing.chen@utoronto.ca (J. M. Chen).*

[1] *Joint first authorship.*

Abstract

An accurate estimation of forest canopy gap fraction (GF) is a prerequisite for remote sensing retrievals of several associated canopy parameters e.g. leaf area index, fAPAR (fraction of photosynthetically

active radiation absorbed by the canopy), clumping index, etc. A universal canopy GF model for forests is required for various tree distribution patterns on flat and slopping terrains, yet existing models so far do not possess all these abilities simultaneously. For example, the Neyman type-A model, the Poisson model, and the hypergeometric model are suitable only to forests with clumped, random, and regular tree distributions, respectively. In this regard, the suite of Nilson's canopy GF models developed for forests with various tree distributions have the potential to become universal models. For this purpose, this study attempts to overcome the following limitations of these models to make them be true universally applicable: (1) canopy GF calculated by the Nilson's models is mostly accurate for various tree distributions at nadir whereas at off-nadir, it is either underestimated for clumped tree distributions or overestimated for regular tree distributions at off-nadir. And (2) Nilson's models were developed for flat terrains and untested for sloping terrains. Herein, two Nilson's models are modified by expanding the calculation of overlap among crowns (OAC) at nadir to the whole hemispherical space. The results show that all canopy GF simulations in the new models (New91 and New99) show higher consistency with ray-tracing results than those in original Nilson's models in all directions, highlighting the need to consider directional OAC. The modified models (especially for New99) are suitable for various tree distributions on flat and slopping terrains and therefore increased the universality of the original Nilson's models suitable for a wide-range of remote sensing applications. New99 can be deemed as a universal canopy GF model for forests with various tree distributions.

Keywords

Forest canopy gap fraction, universal model, directional overlaps among crowns, Nilson's models, tree

distribution

1 Introduction

Canopy gap fraction (or frequency, GF) is defined as the probability of the transmission of a light beam passing through the canopy (Nilson, 1971). The material of this over-story layer differs from the material of the understory in regard to the spectral and structural properties. Therefore, canopy GF is essential in determining light absorption and multiple scattering effects within the medium (Yin et al., 2020). Canopy GF is also a fundamental parameter to support *in situ* leaf area index (LAI) measurements based on several optical instruments (e.g., LAI-2000 and digital hemispherical photography) (Jonckheere et al., 2004; Weiss et al., 2004), also physically-based canopy reflectance models (Widlowski et al., 2015; Kuusk, 2018). Canopy GF also supports retrieval of biophysical variables, e.g., fAPAR (fraction of photosynthetically active radiation absorbed by the canopy), LAI, and clumping index (Myneni et al., 1997; Knyazikhin et al., 1998; Roujean, 2002; Chen et al., 2005; Gonsamo et al., 2011; Jiao et al., 2018; Fang, 2021) from canopy reflectance models, either from ground-based or remotely sensed observations.

The definition of the canopy GF model was first issued from the Beer-Lambert theory as follows,

$$P(\theta)=\mathrm{e}^{-G(\theta)L/\cos(\theta)} \tag{1}$$

where $P(\theta)$ is the canopy GF in the direction θ; $G(\theta)$ is defined as the projection of a unit foliage area in the direction θ (Ross, 1981), which is closely related to the leaf angle distribution; L is the LAI, which is most commonly defined as one half the total (all-sided) leaf area per unit ground surface area (Chen and Black, 1992).

An important assumption in the Beer-Lambert theory is that leaves are randomly distributed within the canopy. Yet it is often invalid for forest stands as the majority of foliage aggregates within a single

crown and then crowns at the patch scale of the forest. The pattern of the distribution can be clumped, random, or regular. Clumped distributions often occur in coniferous forests with within-crown and between-crown gaps depending on crown shape. For such, the Beer-Lambert theory was later modified and is today considered in the following form,

$$P(\theta)=\mathrm{e}^{-G(\theta)L\Omega/\cos(\theta)} \tag{2}$$

where Ω is a correction coefficient, first introduced by Nilson (1971), commonly referred as the clumping index or Nilson's coefficient. It is indeed a fundamental parameter to describe the level of leafy material aggregation, relative to the random case (i.e., the Poisson model).

The function of forest depends on tree spatial arrangement, which has an impact on their growth and protection (Diggle, 2013; Illian et al., 2007). The distribution of trees in a forest, either natural or forced, is closely linked to canopy GF which depends on the overlap among crowns (OAC). It has been widely studied in ecology, i.e., quantitative ecology, community ecology, and landscape ecology, and numerous indexes were proposed to provide quantitative description of tree distributions (Law et al., 2009; Lang et al., 2021). This led to different scenarios (clumped, random, and regular) that have impacts on the radiation and mass exchanges of forests (Illian et al., 2007; Geng et al., 2021). Assuming randomness of natural resources, e.g., water and soil nutrients, a random tree distribution was often adopted for forest canopies for calculating canopy GF and modeling canopy reflectance (Li and Strahler, 1985; Rosema et al., 1992; Chen and Leblanc, 1997; Wenge Ni et al., 1999; Atzberger, 2000; Fan Weiliang et al., 2014; Geng et al., 2017; Wu et al., 2019a; Geng et al., 2022b). The Poisson distribution is the model for this purpose by default and in general its reliability is verified first (Fan et al., 2015; Wu et al., 2019b). Yet the tree distributions were found to show different patterns from the Poisson model in many cases. Chen and and Leblanc (1997) found from their analysis that the trees

distribution often showed clumped, patchiness, cluster, or aggregated scenarios at large scales. They used the Neyman type-A model instead of the Poisson model to describe the tree distribution at coarse scales. The Neyman type-A model is also known as the double Poisson model because two random processes are used in this model: trees are assumed to be randomly distributed in clusters with a randomly distributed cluster size (or the tree number in the clusters), and the centers of the clusters are randomly distributed in space. At small scales (e.g., less than 100 m), more regularity was noticed for the tree distribution rather than random or clumped. Geng et al. (2016, 2017) recently presented a hypergeometric model to confirm such regularity in tree distributions at fine scales. These authors deemed that each crown had a "private space" that could not be occupied by other crowns. Similar work has also been performed by (Goel and Thompson, 2000).

Aforementioned canopy GF models have been widely used for calculating forest canopy GF and modeling canopy BRF (Bidirectional Reflectance Factor). However, each of them has their own domains of application. For instance, the Neyman type-A model cannot be considered for forests with regular tree distributions. Randomness is a common feature of natural forests while the regularity and patchiness are more easily shown in forest plantations. Some particular tree distributions (e.g., line-shape) with the particular orientations and azimuthal effects are common to forest plantations that facilitate efficient managements, i.e., irrigation, fertilization, drainage, and harvest, especially for productive forests and orchards. In fact, the tree distribution may show various alternatives and the theoretical canopy models rarely satisfy entirely to a full description of tree distributions at multiple spatial scales and for different types of management.

Two Nilson's generic canopy GF models based on the Fisher's group index (GI) were proposed to describe various tree distributions in forests (e.g. Nilson, 1999; Nilson and Peterson, 1991). GI captures

the essence of canopy GF calculation: OAC. These authors considered two key parameters, i.e. crown closure and canopy closure, to describe OAC and calculate canopy GF. The models were validated with *in situ* measurements and further introduced as a key module in many forest canopy reflectance models (Nilson and Peterson, 1991; Kuusk, 1995; Kuusk and Nilson, 2000; Kuusk, 2001). Note that crown closure and canopy closure are only used at nadir in Nilson's models, leading to canopy GF might be incorrectly calculated at off-nadir. The aim of this study is to improve Nilson's canopy GF models by constructing a more general and accurate forest canopy GF model applicable to various tree distribution patterns resulting from natural and managed forest on flat and slopping terrains.

2 Theory

2.1 Forest canopy GF models and tree distribution patterns

1) Poisson model for forests with random tree distribution

Based on the randomness of natural resources, e.g., water and soil nutrients, a random tree distribution was usually considered for forest canopies when considering canopy GF and reflectance models (Li and Strahler, 1985; Wenge Ni et al., 1999; Wu et al., 2019a). The canopy GF ($P_{Poisson}$) considering opaque crowns led to the next expression:

$$P_{Poisson}(\theta)=\left(1-\frac{t_c(\theta)}{S(\theta)}\right)^n \tag{3}$$

where n is the number of tree in the forest stand, $t_c(\theta)$ is the crown projected area in the view direction θ, and S is the stand area, and $S(\theta)$ is the stand projected area in the θ, calculated by $S(\theta)= S \bullet \cos(\theta)$ (Geng et al., 2022b). After considering GF within an individual crown (e.g., translucent crowns), canopy GF can be expressed as follows,

$$P_{Poisson}(\theta)=\left\{1-\frac{t_c(\theta)\cdot[1-p_c(\theta)]}{S(\theta)}\right\}^n \quad (4)$$

where $p_c(\theta)$ is the GF of an individual crown (known as crown GF) in the direction θ, and can be expressed as follows (Fan Weiliang et al., 2014; Nilson, 1999),

$$p_c(\theta)=e^{-G(\theta)\cdot L_c/t_c(\theta)} \quad (5)$$

where L_c is the leaf area within an individual crown. If the crown projected area in the view direction $t_c(\theta)$ is obviously smaller than stand projected area $S(\theta)$, the Eq. 5 can be rewritten as the exponential form, and canopy GF can be calculated as follows (Geng et al., 2022a),

$$P_{Poisson}(\theta)=e^{-t_c(\theta)\cdot[1-p_c(\theta)]/S(\theta)} \quad (6)$$

Similar work was performed in using the horizontal plane as a projected plane (e.g. Nilson, 1999). In this study, we used the view perpendicular plane (VPP, the plane is perpendicular to the view direction) rather than horizontal plane to calculate canopy GF, i.e., the stand and all crowns projected in the VPP rather than horizontal plane. For calculating canopy GF, the transition from the horizontal plane to the VPP is equivalent and was widely applied in the literature (Fan Weiliang et al., 2014; Fan et al., 2015; Geng et al., 2016a).

2) Neyman type-A (double Poisson) for forests with clumped tree distributions

The Neyman type-A model was reported to be appropriate to describe the clumped tree distribution (Chen and Leblanc, 1997). In this model, trees are assumed to be randomly distributed in each cluster of the model, and the size (tree number) and position of cluster are randomly distributed. Canopy GF (P_{Neyman}) can be written as follows (Chen and Leblanc, 1997):

$$P_{Neyman}(\theta)=\sum_{i=1}^{k}P_{tj}(V_g)p_{\text{gap}}^{j}(\theta)+P_{t0} \quad (7)$$

where, k is the maximum number of tree in a quadrat which is a sampling window and its size often less than the forest stand (e.g.,100 m × 100 m), and

$$P_{ij}(V_g) = \sum_{i=1}^{k} P_N(i) \frac{(i+j-1)!}{(i-1)!\,j!} [1 - \frac{V_g}{A}]^i [\frac{V_g}{A}]^j \quad (8)$$

$$P_N(i) = \mathrm{e}^{-m_1} \frac{m_2^i}{i!} \sum_{j=1}^{\infty} [m_1 \mathrm{e}^{-m_2}]^j \; j^i / j! \quad (9)$$

where j is the cluster number in each quadrat, and i is the tree number in each cluster; m_1 and m_2 are mean value of j and i, respectively. The larger value of m_2, the more clumped tree distribution is. If it is close to zero, then the tree distribution turns to be close to the Poisson model. P_N is the Neyman probability of finding i trees in a quadrat. The Neyman type-A model describes a double-random process, thus it is also called "double Poisson" model. The main difference between the Poisson model and the Neyman type-A model relies on the probability to find i trees in a quadrat meeting the Neyman type-A model rather than the Poisson model. The variance of i of the Neyman type-A model is generally larger than that of the Poisson model.

3) Hypergeometric model for forests with random and regular tree distributions

Both randomness and regularity of tree distribution are concurrent, assuming there exists an exclusion zone around a single tree. The hypergeometric model describes such randomness and regularity of tree distribution: each crown has its "private space" and cannot be occupied by other crowns and crowns can only randomly distribute in "non-private space" of other crowns rather than any where. An important distance parameter RASD, defined as the relative allowable shortest distance between centers of two adjacent crowns divided by the mean diameter of the crowns, is used to describe the exclusion distance among trees and the regularity of tree distribution. The larger RASD, the more regular tree distribution is. When RASD = 0, it means there is no exclusion distance among

trees and no "private space" for trees, indicating trees meet the Poisson model. Then, canopy GF (P_{Hyper}) can be calculated as follows (Geng et al., 2016a),

$$P_{Hyper}(\theta)=\sum_{i=1}^{n}\left[1-\frac{t_c(\theta)(1-p_c(\theta))}{S(\theta)-S_{real\_excl\_p}(\theta)(1-p_c(\theta))(i-1)}\right]^i \tag{10}$$

where, $S_{real\_excl\_p}$ is the projected real exclusion area (Geng et al., 2016a).

The main difference between the Poisson model and the hypergeometric model is the exclusion area for each crown (denominator in Eq. 10), indicating there is a "private space" for each crown which cannot be occupied by other crowns. This yields the basic principle of the hypergeometric model (Geng et al., 2016a, 2022a).

4) Nilson's canopy GF model for forests with various tree distributions at multiple spatial scales

Aforementioned canopy GF models of tree distribution rely on some necessary assumptions, which places a limit in their applications. For instance, the Poisson and the Neyman type-A model are not applicable for forests with regular distributions. Nilson and Peterson (1991) presented a relatively "universal" canopy GF model which is based on the Poisson model but using a Fisher's group index (GI), defined as the relative variance of the number of trees in the single tree projected area (Nilson, 1999). It serves to describe various tree distribution patterns. The canopy GF ($P_{Nilson91}$) is expressed as follows (Nilson and Peterson, 1991),

$$P_{Nilson91}(\theta)=\mathrm{e}^{-(1-p_c(\theta))c_B C_{CR} K(\theta)} \tag{11}$$

where C_{CR} is the crown closure, defined as the sum of crown projections per unit ground area, whereas the overlapped regions of crown projections have been multiply counted, considering the amount of overlapping tree crowns, calculated by the sum of crown projections per unit ground area at nadir. C_{CAN} is the canopy closure, defined as relative ground area occupied by tree crowns, overlapped regions counted only once, and calculated by one minus the between-crown GF at nadir. The difference

between the two closures is that overlapped regions of crown projections have been multiple counted for the former one, yet overlapped regions counted only once for the latter one. $K(\theta)$ describes the relative change of projection area along with a change in the view direction θ and thus characters the crown form, and c_B is a tree distribution pattern parameter that can be derived from GI. c_B, C_{CR}, C_{CAN}, and $K(\theta)$ can be expressed as follows,

$$c_B = (-\ln \mathrm{GI})/(1-\mathrm{GI}) \tag{12}$$

$$C_{\mathrm{CR}} = Nt_a(0) \tag{13}$$

$$C_{\mathrm{CAN}} = 1-\mathrm{e}^{-c_B C_{\mathrm{CR}}} \tag{14}$$

$$K(\theta) = \sqrt{1+(h/2R)^2 \tan^2\theta} \tag{15}$$

Nilson (1999) presented another forest canopy GF ($P_{Nilson99}$) model using the tree distribution parameter c instead of c_B. Viz:

$$P_{Nilson99}(\theta) = \mathrm{e}^{-c(\theta)C_{CR}K(\theta)} \tag{16}$$

$$c(\theta) = \frac{-\ln[1-(1-p_c(\theta))(1-\mathrm{GI})]}{1-\mathrm{GI}} \tag{17}$$

As the universal tree distribution parameter GI is used in Nilson's models, such category of models is not restricted to a certain tree distribution and is deemed to be a relatively universal forest canopy GF model. This is the main difference between the above-mentioned three models (the Poisson, the Neyman type-A, and the hypergeometric models) and the two Nilson's models (Nilson91 and Nilson99).

5) New Nilson's canopy GF models considering the directional OAC

It is widely known that canopy GF is strongly influenced by both crown GF (i.e., p_c in Eq. 5) and OAC. As matter of fact, it is necessary to consider both directional OAC and crown GF to accurately

calculate directional canopy GF. Note that the tree distribution parameters GI, c_B, and c are considered at nadir or on horizontal ground in the two Nilson's models. For off-nadir angles, the tree distribution parameters GI and c are also the same to the nadir direction, and OAC is mainly influenced by $K(\theta)$ in the two Nilson's models (Eq. 11, 16). However, $K(\theta)$ is only related to crown size rather than the tree distribution parameter as shown in Eq. 15, thereby indicating that the tree distribution parameters are not used to calculate canopy GF at off-nadir. For instance, $K(\theta)$ is only related to the zenith angular crown projected area $p_c(\theta)$ in Eq. 15. It means that the spatial relationship among trees and OAC at off-nadir are simplified, leading to that canopy GF at off-nadir might be incorrect.

The directional OAC differs from Nilson's canopy GF models which consider only tree distribution parameters at nadir to describe OAC. It remains available for the whole hemispherical space, leading to the modifications of Eq. 11 and 16 of Nilson's canopy GF models as follows:

$$P_{New91}(\theta) = \mathrm{e}^{-(1-p_c(\theta))c_B'(\theta)C_{CR}'(\theta)} \tag{18}$$

$$P_{New99}(\theta) = \mathrm{e}^{-c'(\theta)C_{CR}'(\theta)} \tag{19}$$

where,

$$c_B'(\theta) = (-\ln \mathrm{GI}'(\theta))/(1-\mathrm{GI}'(\theta)) \tag{20}$$

$$c'(\theta) = \frac{-\ln[1-(1-p_c(\theta))(1-\mathrm{GI}'(\theta))]}{1-\mathrm{GI}'(\theta)} \tag{21}$$

$$C_{\mathrm{CAN}}'(\theta) = 1-\mathrm{e}^{-c_B'(\theta)C_{\mathrm{CR}}'} \tag{22}$$

$$C_{\mathrm{CR}}'(\theta) = Nt_c(\theta) \tag{23}$$

where, the subscript 'New91' is a modification of Nilson91, and 'New99' is a modification of Nilson99 considering the directional OAC (i.e., directional C_{CR} and C_{CAN} rather than only C_{CR} and C_{CAN} at nadir). The superscript '' means directional parameter corresponding to the same parameter in the two Nilson's models to consider the directional OAC rather than OAC only at nadir. Although zenith angle θ exists in the tree distribution parameter c in Eq. 17, c is only related to the crown projected area

rather than the directional OAC. The main difference between the new models and the previous Nilson's models is that the calculation of OAC with the tree distribution GI is expanded from nadir direction to the whole hemispherical space, i.e., C_{CR} and C_{CAN} are calculated in different view directions rather than constants in all directions, and the directional OAC instead of $K(\theta)$ is used to calculate directional canopy GF. After the above processes (i.e., Eq. 18-23), both directional OAC and crown GF arc considered accurately in the two new models to calculate directional canopy GF.

3 Methods

To show the universal applicability of the new canopy GF models, different types of forests with a variety of tree distribution patterns on horizontal and sloping terrains at different spatial scales are considered here. The scenarios of exclusion distances among trees, stand orientation or azimuth effect, spatial scale effects, and slope effects are considered to encompass complex realistic cases.

Generally, tree distribution patterns in reality can be divided into three main kinds: clumped, random, and regular. According to the theories in the Neyman type-A model, the Poisson model, and the hypergeometric model, six forest stands with clumped, random, and regular tree distributions are generated based on these three models as shown in Figure 1, including a forest stand with clumped tree distribution (Neyman type-A distribution with m_2 = 3), a stand with the Poisson distribution, three stands with regular distributions (the hypergeometric distributions with RASD = 0.5, 1, 1.15, and 1.25 (the maximum RASD), and the stand name refers to HG1, HG2, HG3, and HG4, respectively). Forest canopy coverage is closely related to tree distribution. For example, the low canopy coverage, between-crown gaps or large space are conspicuously seen in the forest stand with the clumped tree distribution, leading to a strong heterogeneity of forest canopy or a region in the stand. In contrast, the high canopy coverage, between-crown gaps are shown in the forest stands with regular tree

distributions, especially in forest stands with RASD > 1 (i.e., Figure 1 (d-f)). It is due to the different OAC among these forests. All parameters in these forest stands are the same except for the tree distribution and canopy coverage. For detailed information of forest stand parameters, please see Table 1.

The assumption of azimuthal isotropy may be workable for natural forests, yet it is often invalid for forest plantations. Forest plantations with significant orientations and azimuth effects are considered in this study. Forests plantations with four line-shape (LS) and four column-shape (CS) tree distributions are exemplified in Figure 2. The azimuth effect of stand is considered by rotating the stand azimuth angle 90° and tree distributions transit from LS to CS.

The spatial scale effect is considered here. The area of the above forest stands are the same (40 × 40 m^2), i.e., at the same spatial scale. Combining four forest stands in Figure 1 and Figure 2 to form two large forest stands A and B (80 × 80 m^2) to evaluate the new models at large scales (as shown in Figure 3).

In addition, the sloping effect is also considered in this study. The vertical coordinates value of crowns meet $Z = \tan(\alpha) \cdot X$. Where X is x coordinate value of crowns, Z is the vertical coordinates value of crowns, and α is the slope. Here $\alpha = 30°$. The horizontal positions of trees on sloping terrains are identical to those on horizontal surface to keep the same tree distributions at nadir.

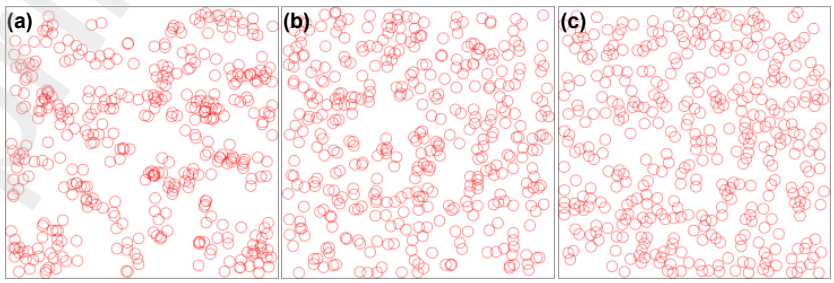

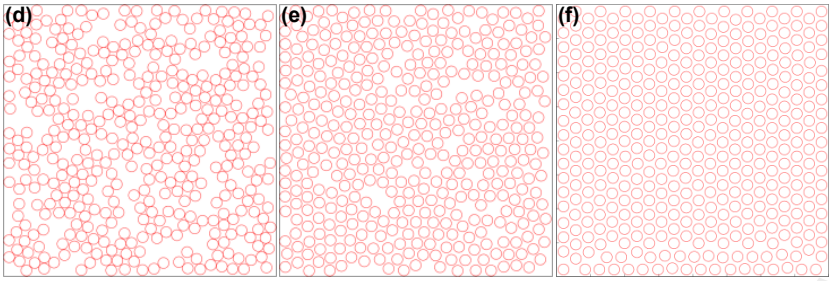

Figure 1. Comparisons of forests with the same tree density but different tree distribution patterns (from clumped to random to regular. ((a): Neyman; (b): Poisson; (c): HG1 (RASD = 0.5); (d): HG2 (RASD = 1); (e): HG3 (RASD = 1.15); (f): HG4 (RASD = 1.25)).

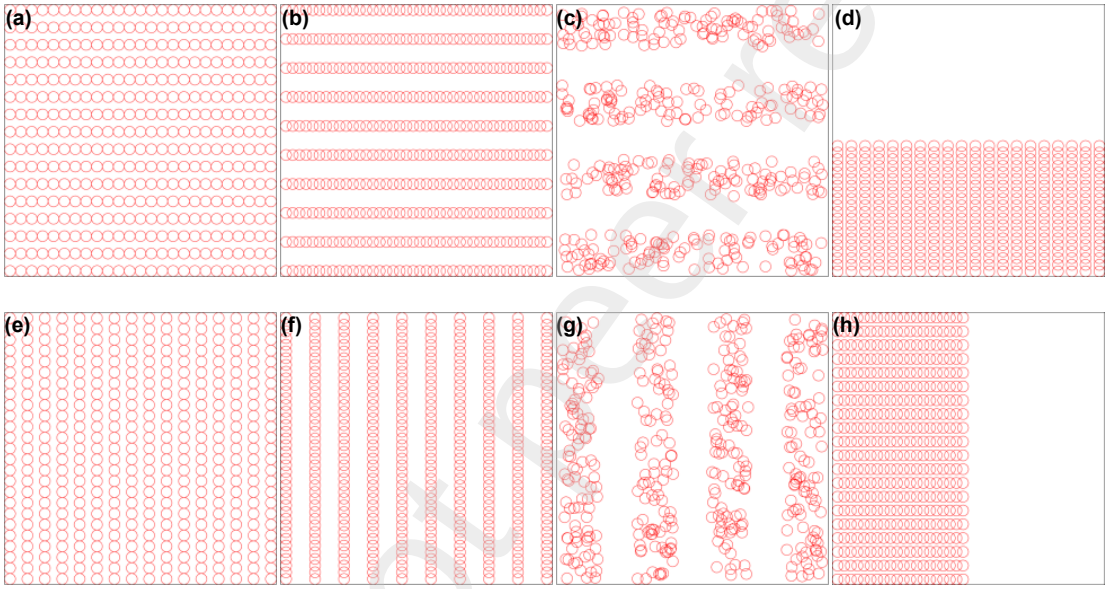

Figure 2. Comparisons of forests with the same tree density but different managements and stand azimuth angles (orientations). (((a)- (d): LS1- LS4; (e)- (h): CS1- CS4). (e-h) is 90° rotation of (a-d) from LS to CS, respectively).

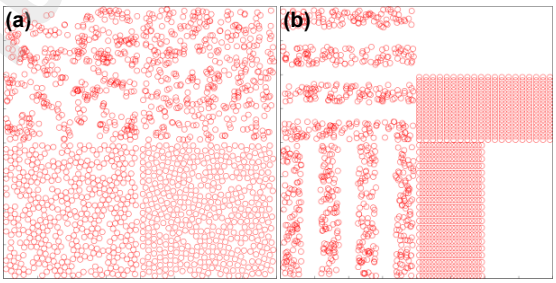

Figure 3. Combinations of forest stands in Figure 1 (a,b,d, and e) and Figure 2 (c,d,g, and h) to construct two large forest stands A (a) and B (b).

Table 1. Stand parameter values.

Parameter	Value
Stand area (m^2)	40×40
Tree density (trees/ha)	2500
Crown shape	Ellipsoid
Crown radius (m)	0.8
Crown height (m)	3
LAI	3
Leaf angle distribution	Spherical
Tree distribution	Neyman, Poisson, HG1-4, LS1-4, CS1-4
Coverage (%)	34, 38, 42, 50, 50, 50, 50, 37, 34, 37

4 Results

Here, a ray-tracing (RT) method is used to validate the canopy GF simulations in the two new models (New91 and New99). The variations of canopy GF with view zenith angle (VZA) in forests with various tree distribution patterns, azimuth effects, spatial scale effects, and sloping effects are shown here to show the universality and accuracy of the new models.

We used the relative error (RE, calculated as follows) to appraise the accuracy of the simulations.

$$RE = (S_{imulation} - R_T)/R_T \quad (24)$$

where $S_{imulation}$ is canopy GF simulation in the two previous Nilson's models (Nilson91 and Nilson99) and two new models (New91 and New99)), and R_T is canopy GF result of RT method.

4.1 Forests with various tree distribution pattern effects

Figure 4 shows the results of cross-comparison between simulated canopy GF by the four canopy GF models and RT method. Table 2 shows the mean RE in canopy GF results of the two Nilson's canopy GF models and two new models in forests with different tree distribution patterns. There is no obvious difference between Nilson91 and Nilson99 results. As only closure at nadir is considered in the previous two Nilson's models, the canopy GF curves in Figure 4 show similar values and trends. Especially, the canopy GF results in the Nilson91 and Nilson99 are identical in all forests with the

same canopy closure (the canopy closure is equal to 50% for stands from Figure 1 (d) to (f) because there is no OAC at nadir in these forests).

All canopy GF simulated by the Nilson91 and Nilson99 at nadir show high consistency by the RT results in all forest stands. The mean RE in the two Nilson's models and two new models in all directions (calculated by the averaged absolute values of RE in all directions) is less than 10% for the forests with the Poisson model and HG1 tree distributions. It means that all those models have the ability to simulate canopy GF at nadir for forests with the Poisson tree distribution or closed to the Poisson tree distributions.

However, the REs in the two Nilson's models increase for other forests at off-nadir as shown in Figure 4 and Table 2. Generally, canopy GF simulated by the Nilson91 and Nilson99 models are underestimated for the forests with the Neyman-A tree distribution (Figure 4 (a)), and overestimated for the forests with the hypergeometric tree distributions with large RASD (Figure 4 (d-f)) at off-nadir. The mean RE reaches up 46% for Nilson99 and 37% for Nilson91, and the maximum RE in all directions reaches up to 144% for Nilson99 and 90% for Nilson91 in the HG4 stand at large zenith angles. In contrast, the canopy GF simulations in the two new models are consistent relatively well with the RT results, especially for New99. There is no notable difference in canopy GF results between New99 and RT in most directions for most forest stands. For instance, the mean RE for New99 are low by 3% in the Neyman, the Poisson, and the HG1 stands. This sustains the effort for considering OAC in off-nadir directions in the new models.

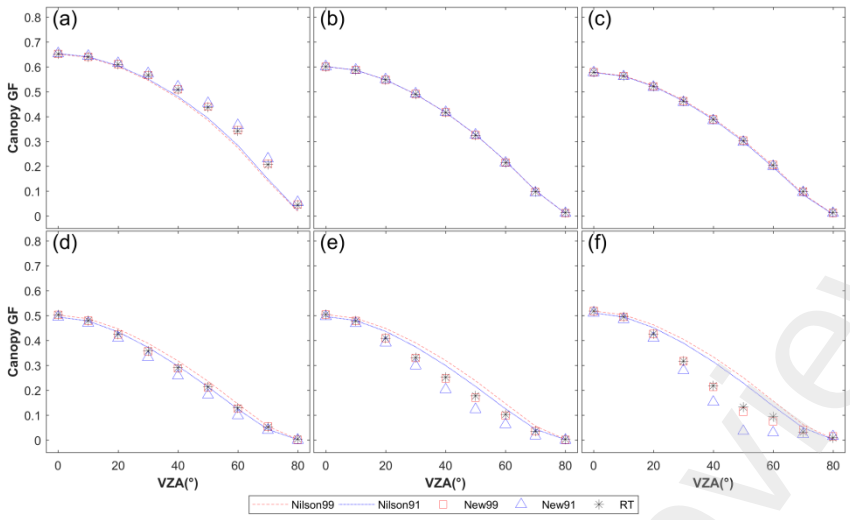

Figure 4. Comparisons of canopy GF at various zenith angles in forests with different tree distributions (corresponding to Figure 1, (a): Neyman; (b): Poisson; (c): HG1(RASD= 0.5); (d): HG2(RASD= 1); (e): HG3(RASD= 1.15); (f): HG4(RASD= 1.25)).

Table 2. Mean RE in canopy GF results between the four canopy GF models and RT in forests with different distribution patterns (%).

Stand	Nilson99	Nilson91	New99	New91
Neyman	15	13	1	6
Poisson	4	4	2	3
HG1	7	8	2	4
HG2	9	10	10	22
HG3	25	15	11	30
HG4	46	37	16	34

4.2 Forests with orientation or azimuth angle effects

Figure 5 shows the zenith angular variations of canopy GF in the forest plantations with particular orientations or azimuth angles. The zenith angular variations of canopy GF are similar to those in Figure 4. Those variations show different features with the RT results to some extent although canopy GF shows a decrease with an increment of zenith angle in all forest stands.

As there is no azimuth dependence in the two Nilson's models, canopy GFs in stands with different

orientations or azimuth angles are identical (e.g., canopy GF simulations in the two Nilson's models in Figure 5 (b) and (f)). This leads to the notable differences in canopy GF between the two previous models and RT. Table 3 shows the mean RE in canopy GF results between the four canopy GF models and RT. The mean REs of two previous Nilson's models are larger than 25% for almost all forest stands except for the stand LS3, especially for the stand LS2 (the mean REs are greater than 390% for the two Nilson's models). The canopy GF simulations also show high consistency with the RT results (the mean REs are less than 15% in all forest stands). In this regard, the azimuth problem in the previous two models is solved in the new models.

Similarly to the results in Figure 4, directional canopy GF simulations in two Nilson's models are overestimated in the directions where large between-crown gaps appear (meaning clumped distribution), but underestimated in the directions where tree distributions show regular distribution. Here, we prefer to use a directional tree distribution rather than nadir tree distribution to describe the directional canopy GF because the latter is insufficient to describe the directional OAC and to calculate directional canopy GF as shown in Figure 5.

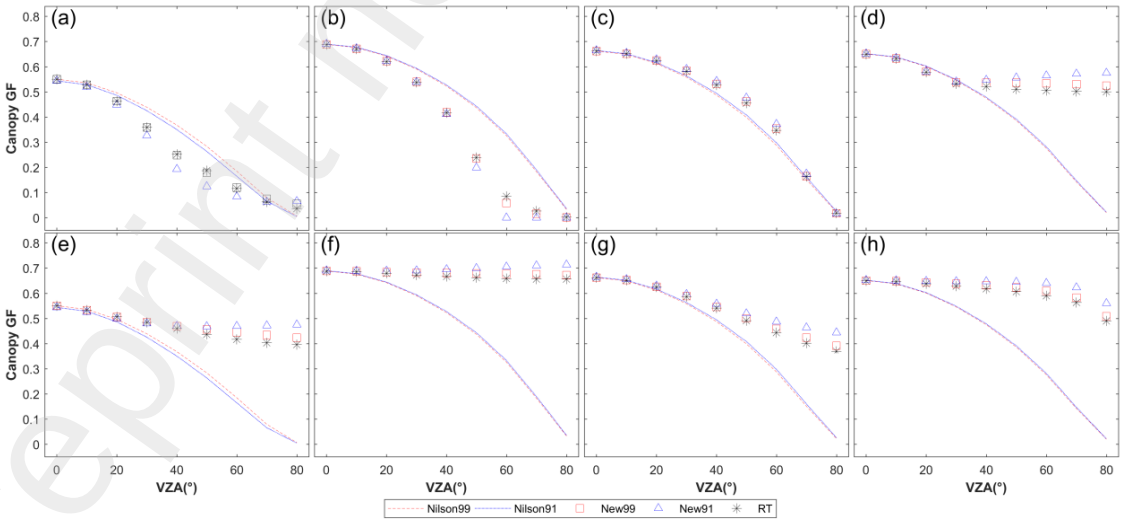

Figure 5. Comparisons of canopy GF at various zenith angles in forests with different stand orientations or azimuth angles (corresponding to stands in Figure 2, (a)- (d): LS1- LS4; (e)- (h): CS1- CS4).

Table 3. Mean RE in canopy GF between the four canopy GF models and RT in forests with different stand orientations or azimuth angles (%).

Stand	Nilson99	Nilson91	New99	New91
LS1	35	28	10	21
LS2	393	421	14	37
LS3	9	9	2	4
LS4	30	30	3	7
CS1	35	38	3	8
CS2	34	34	2	5
CS3	27	26	2	7
CS4	36	35	2	6

4.3 Forests at different spatial scales

The total canopy GF in two large forest stands (Figure 3) calculated by the two Nilson's models and two new models are shown in Figure 6 (1). In addition, we averaged the canopy GF in each sub forest stand to compare the total canopy GF in the two large forest stands (Figure 6 (2)).

For the large stand-A (Figure 3 (a) and Figure 6 (a)), all canopy GFs calculated by the two Nilson's models and the new models are generally closed to the RT results. RE is 11%, 13%, 5%, and 8% for Nilson99, Nilson91, New99, and New91, respectively (as shown in Table 4). It means that all four models have abilities to calculate canopy GF for this stand. It is due to that the tree distribution in large stand-A is a compound of that in the four sub-stands. Tree distributions in the large stand-A show more randomness than in HG1 and HG2, and also show more regularity than that in Neyman and Poisson stand.

For the large stand-B (Figure 3 (b) and Figure 6 (b)), canopy GFs calculated by the new models are also generally closed to the RT results (the RE is only 3% and 7% for New99 and New91, respectively), while there are large REs produced by the two Nilson's models (the RE is 28% and 27% for Nilson99 and Nilson91, respectively). Because of the notable space in Figure 3 (b), canopy GF can

not be closed to zero.

There is no obvious difference between total canopy GF in the two large stands and averaged canopy GF in four sub stands as shown in Figure 6, indicating that the canopy GF can be averaged in the sub-stands at this spatial scale.

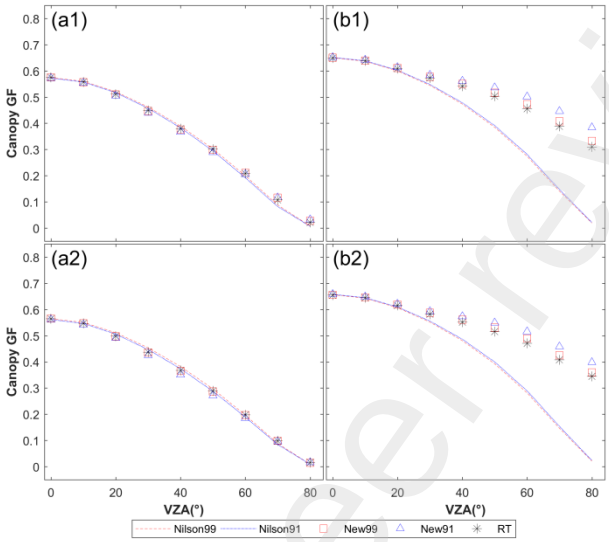

Figure 6. Comparison of simulated canopy GF at large forest stands ((a): combination of four sub-stands in Figure 1 (b,c,e, and f) and (b): combination of four sub-stands in Figure 2 (d,e,h, and i); (1): Total canopy GF; (2): averaged canopy GF in four sub stands).

Table 4. Mean RE in canopy GF results between the four canopy GF models and RT in two large forest stands (%).

Stand	Nilson99	Nilson91	New99	New91
Larger stand-A	11	13	5	8
Larger stand-B	28	27	3	7

4.4 Forests at different sloping terrains

Sloping terrains change the canopy structure and distort the view inclination angle of canopy. As OAC can be calculated correctly at nadir but simplified at non-nadir in two Nilson's canopy GF models, OAC might be described incorrectly for forests on sloping terrains in these models. The

negative values in abscissa in Figure 7-8 mean that the relative view azimuth angle between aspect is zero, i.e., seeing from the down-slope directions. On the contrary, the positive values in abscissa in Figure 7-8 mean seeing from the up-slope directions.

All canopy GFs at nadir are simulated well by the two Nilson's models as mentioned above. However, all canopy GFs in these two models are symmetrical between down-slope and up-slope directions, indicating that the previous two models were developed for forests on horizontal ground without considering slope effects. It is easily understood because two important OAC parameters forest crown closure C_{CR} and canopy closure C_{CAN} are only related to the stand and crown projected area at nadir ($S(0)$ and $t_c(0)$) rather than off-nadir in the two Nilson's models. Canopy GFs are simulated well for the horizontal forest stand with the Poisson tree distribution as shown in Figure 4(c), while there are non-negligible errors for the forests with the Poisson tree distribution on sloping terrains as shown in Figure 7(c). In addition to Figure 7(c), the mean REs in canopy GF between the two Nilson's models and RT are in fact notable for all forests on sloping terrains. Canopy GFs simulated by these two Nilson's models are obviously underestimated in the down-slope directions (negative values of VZA in Figure 7-8) in all forest, but overestimated in the up-slope directions (positive values of VZA in Figure 7-8) in most forest stands (except for LS4, CS1, CS3, and CS4, i.e., Figure 8 (d), (e), (g), and (h)). The REs produced by the two Nilson's models increase from clumped tree distributions (Figure 7 (a)- (b)) to regular distributions (Figure 7 (d)-(f)) in the up-slope directions, but decrease in the down-slope directions.

However, the mean REs in canopy GFs between the new models and RT are generally lower than 10% in most directions, indicating the ability of the new models in simulating canopy GF for forests with various tree distributions on sloping terrains, especially for New99. It means that the directional

OAC and canopy GF are calculated well in both new models, especially for New99.

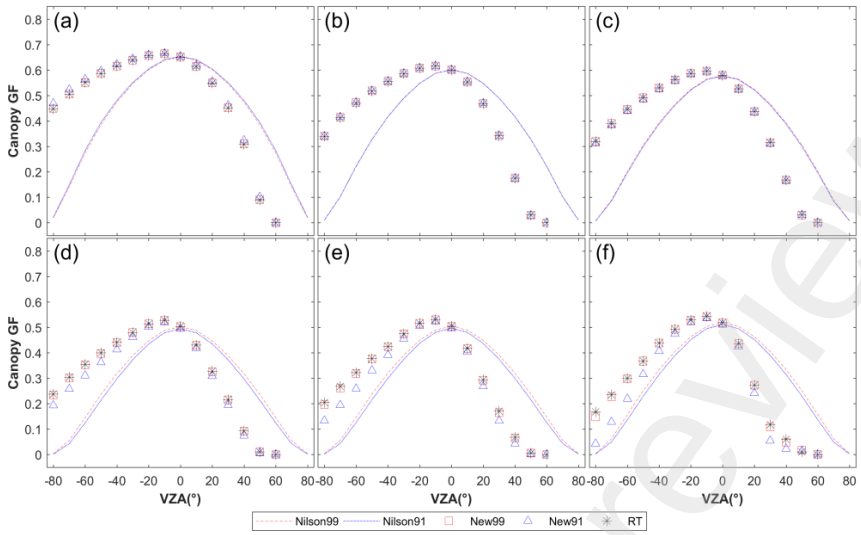

Figure 7. Comparison of simulated canopy GF at various zenith angles and in the different forests on sloping terrains (slope = 30°) corresponding to Figure 1 ((a): Neyman; (b): Poisson; (c): HG1 (RASD= 0.5); (d): HG2 (RASD= 1); (e): HG3 (RASD= 1.15); (f): HG4 (RASD= 1.25)).

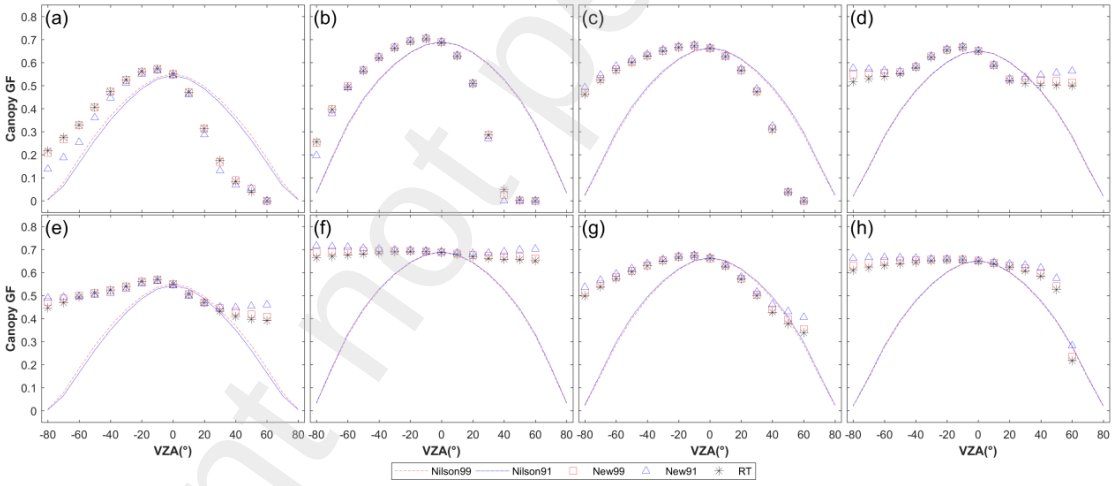

Figure 8. Comparison of canopy GF at various zenith angles and in the different forest stands on sloping terrains (slope = 30°) corresponding to stands in Figure 2. ((a)- (d): LS1- LS4; (e)- (h): CS1- CS4).

5 Validation

5.1 Two forest stands in RAMI platform

Two forest stands inherited from the RAdiative transfer Model Intercomparison exercise (RAMI) are

handled here to validate the results: (1) HET-14 (https://rami-benchmark.jrc.ec.europa.eu/_www/phase/phase_exp.php?strTag=level2&strNext=meas&strPhase=RAMIIV&strTagValue=ACT_WCO). It is a forest plantation of a 9 years old citrus orchard located in Wellington, South Africa (33°36′S, 18°56′E). The scene is based on data provided on courtesy of Jan Stuckens, Ben Somers and colleagues (from the Katholieke Universiteit Leuven in Belgium) who carried out a detailed measurement campaign at this site in 2006/2007. Trees in the HET-14 stand show notable column shape and the stand shows obvious azimuth effect. (2) HET-20 (https://rami-benchmark.jrc.ec.europa.eu/_www/phase/phase_exp.php?strTag=level3&strNext=meas&strPhase=RAMIIV&strTagValue=ABS_HET_ANI). It is a forest canopy where sphere crowns meet the hypergeometric distribution (tree distribution shows both randomness and regularity), and there is no obvious azimuth effect of stems. The parameters of these two forest stands are shown in Table 5, and tree distributions are reported in Figure 9. The directional C_{CR} can be calculated by summarizing of all individual crown projected area divided by the ground projected area in a certain direction. The directional C_{CAN} can be measured by image classification (i.e., image binaryzation) as shown in Figure 9.

Table 5. Parameters of two RAMI forest stands.

PARAMETER	HET 14	HET 20
Stand area (m^2)	108.25 × 103.9	100× 100
Tree number	1115	5039
Crown radius	1.55	0.5
Crown height	2.7	1

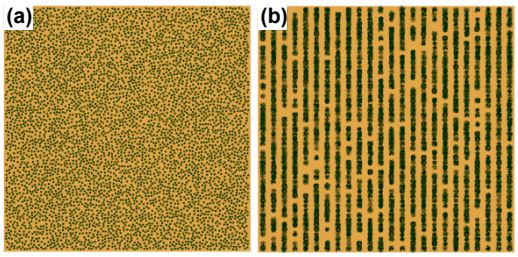

Figure 9. Two forest stands in the RAMI platform ((a) HET-20; (b) HET-14).

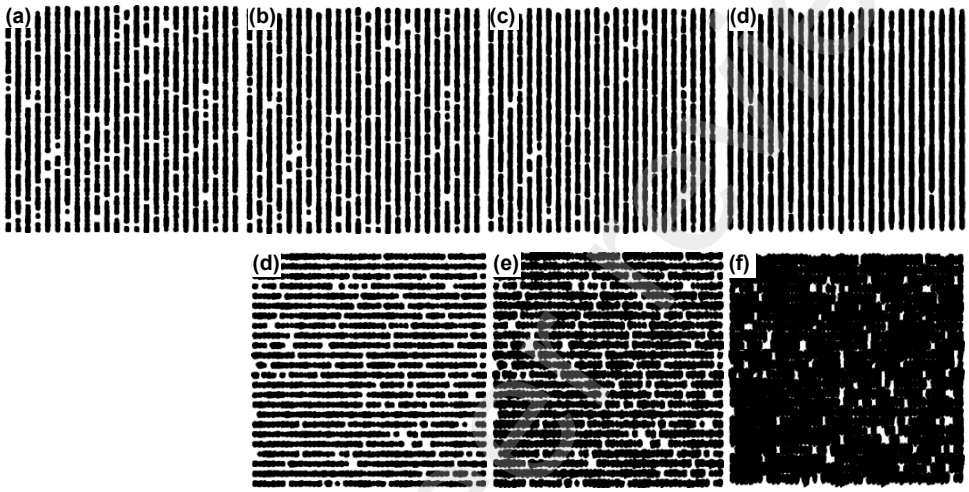

Figure 10. Calculation of directional C_{CR} in the HET-14 forest stand by image binaryzation at different VZAs ((a) VZA= 0°, (b) and (e) VZA=20°, (c) and (f) VZA=40°, (d) and (g) VZA=60°)

Figure 11 shows the comparison of directional canopy GF among different models in different forests. For HET-20 (Figure 11 (a)), all directional canopy GF simulations in the four models are consistent with RT results, validating the ability for all four models. For HET-14 (Figure 11 (b)), canopy GF simulations at nadir in all four models also show good performances with RT results. Generally, directional canopy GF simulations in the two new models show good consistency with RT results. Yet, there are increasing errors in canopy GF between two Nilson's models and RT results with increasing VZA. The errors are closely related to stand azimuth angle. The zenith angular canopy GFs is simplified and azimuth effect was not considered in the two Nilson's models. Because of that, both zenith and azimuth angular canopy GFs can not be calculated accurately in these two models because of the simplifications of directional OAC. Similarly to the gaps between Figure 5 (a-e) and Figure 5 (b-f), canopy GF is underestimated for Figure 11 (b) and overestimated for Figure 11 (c) in the

off-nadir directions, especially at large zenith angles. The error produced by two Nilson's models reaches up to 50% at VZA=60° although the mean RE is lower than 20% (Table 6).

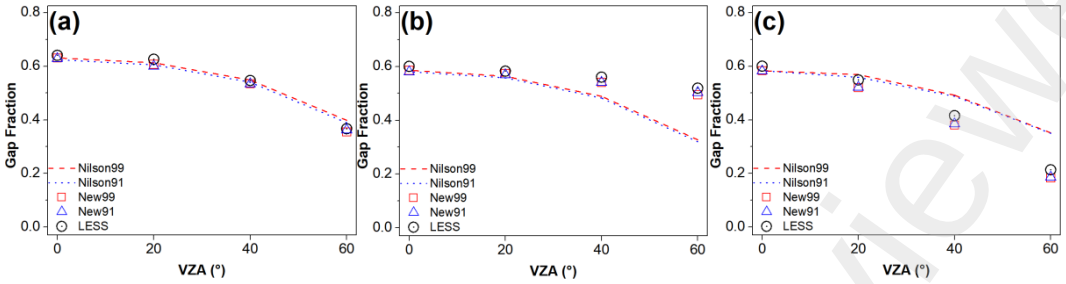

Figure 11. Validation of canopy GF at various zenith angles and in the different forests ((a) HET-20; (b) HET-14; (c) rotating HET-14 from CS to LS).

Table 6. Mean RE in canopy GF between the four canopy GF models and RT in two large forest stands (%).

Stand	Nilson99	Nilson91	New99	New91
HET-20	3	3	2	2
HET-14(CS)	14	15	3	3
HET-14(LS)	19	18	8	7

5.2 A forest stand in Saihanba forest farm

Saihanba forest farm is the largest forest plantation in China. A data-set of point cloud in a 500 m × 500 m forest stand (42°22′54″N, 117°22′39″E - 42°22′39″N, 117°23′01″E, see Figure 12) in the Saihanba forest farm was obtained with an airborne laser scanning (Riegl LMS-Q680i integrated in the CAF-LiCHy system, point cloud density is 10-30 pts/m^2) and a spectral data (Specim AisaEAGLE II, spatial resolution is 0.8m) on 29 August 2018. With the help of these two airborne sensors, individual tree segmentation was completed and forest structures were measured, including tree number (5835), position, and size. For detailed information of experiment design, instruments, and data-set, please refer to (Pang et al., 2021). As the point cloud density was not large enough, LAI might not be retrieved with high precision. Assuming the structures among trees is similar in a forest plantation, leaf area in an individual crown is assumed to be the same and LAI is equal to 4 in the whole image.

Trees in the left part of image (Figure 12 (a)) show relatively regular distribution, while there is an irregular space in the right part of the image. This places a difficulty to describe tree distribution in this image using the Neyman type-A, the Poisson, and the hypergeometric models because of the complexity of tree distribution. Directional C_{CR} can be calculated by summing the crown projected area according to individual tree segmentation results (Pang et al., 2021). Directional C_{CAN} can be calculated by image binaryzation. Directional canopy GF can be accurately simulated in a LESS platform (A 3-D radiative transfer simulation framework large-scale remote sensing data and image simulation (http://lessrt.org)), which provide a batch tool to efficiently calculate canopy GF based on ray-tracing and computer graphics for forests at large scales (Qi et al., 2019).

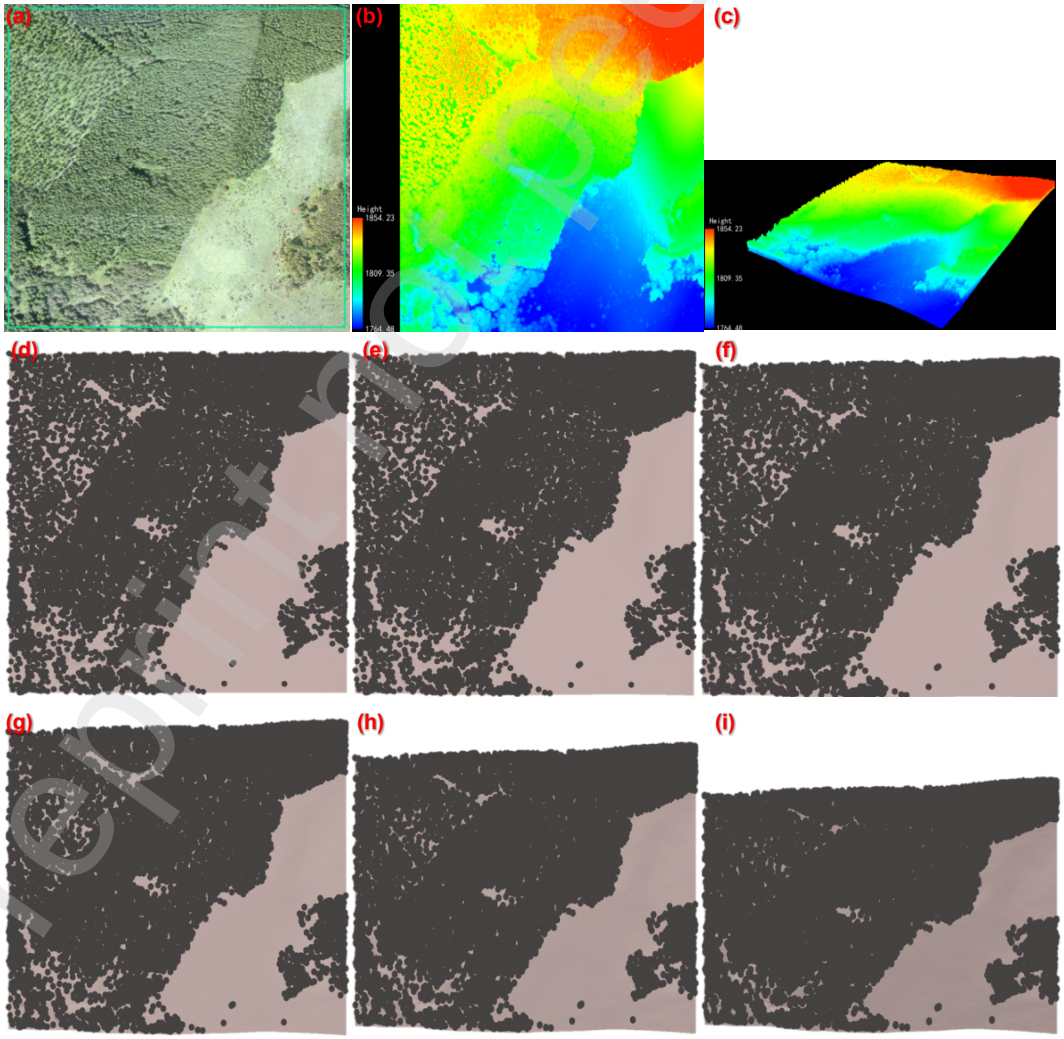

Figure 12. Calculations of directional canopy closures at different VZAs ((a) a high resolution image at nadir; (b) point cloud at nadir; (c) point cloud at off-nadir; (d)-(l) are image for calculating directional canopy closures at 0°-80° with a step of 10°).

Figure 13 show the comparisons of canopy GF calculated by two Nilson's models, two new models, and LESS. Table 7 shows the RE between the simulations and LESS results.

The canopy GF simulations with the two new models are closed to LESS results, especially for New99. Both mean REs are lower than 10%. However, there is a disparity in canopy GF results between two Nilson's models and LESS. Both mean REs in canopy GF between two Nilson's models and LESS are larger than 30%. Although the canopy GF at nadir is simulated well by two Nilson's models, there are notable errors at large VZAs. As existence of an irregular space appears in the image, true canopy GF cannot be closed to zero even at large VZAs (see Figure 12 (j-l)). However, canopy GFs in the two Nilson's model are closed to zero at large VZAs. The results show the deficiency of parameter $K(\theta)$ in Eq. 15. The directional OAC which is closed to the directional tree distribution is not accurately calculated by $K(\theta)$. It is well considered in the two new models, and the results in Figure 13 and Table 7 show the reliability of the two new models, especially for New99.

Compared to the forests in section Results and RAMI, the forest in Saihanba is of more complicated tree distribution and lager area at more complicated sloping terrains. The validation show the accuracy of the new canopy GF models in reality, especially for New99.

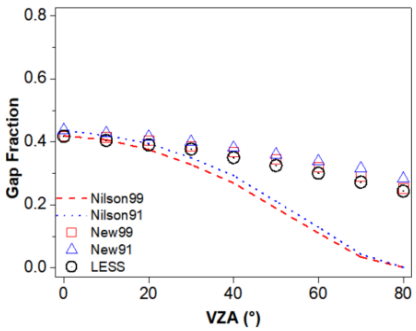

Figure 13. Validation of canopy GF at various zenith angles in a stand in a Saihanba forest stand.

Table 7. Mean RE in canopy GF between the four canopy GF models and LESS in a Saihanba forest stand (%).

Nilson99	Nilson91	New99	New91
40	34	4	9

6 Discussions

6.1 Improvements for previous canopy GF models

Canopy GF is a fundamental and critical parameter in nearly all radiative transfer models because it strongly impacts light interception and the radiation transfer processes within a canopy, and also plays a key role on parameters estimates, such as LAI, fAPAR, bi-directional canopy GF, four components area ratios (known as sunlit foliage, shaded foliage, sunlit ground, and shaded ground), and canopy reflectance or BRF. Therefore, a universal and accurate forest canopy GF is a prerequisite for forward and inverse modeling for diverse forests using remote sensing data. Existing tree distribution models are lacking universality. For instance, the Neyman type-A model was deemed to be suitable for describing clumped tree distributions at large scales (often larger than 250 m). In contrast, the hypergeometric model was reported as being suitable for regular and random tree distributions at small scales (often less than 100 m). The Poisson model is generally suitable for regular tree distributions at the medium scales (e.g., 100 m - 500 m). However, the boundary scales indicated here for these models only provide a rough idea. For instance, a clumped tree distribution could also occur at small scale and

a regular distribution could also arise at broad scale. The Nilson's canopy GF models with a powerful tree distribution parameter GI were reported as being suitable for forests with various tree distributions because GI is deemed as a relatively universal parameter for various tree distributions (Nilson, 1999). OAC at nadir can be accurately expressed by the combination of canopy closure and crown closure at nadir. For instance, the obvious space without any tree cover in Figure 12 can be captured by these two closures. However, OAC was simplified at off-nadir leading to canopy GF at off-nadir might be calculated incorrectly. In addition, Nilson's GF models were presented for forests on horizontal ground. Thus, their applications are inevitably limited.

Results in this study show that the previous two Nilson's canopy GF models show excellent canopy GF simulations for forests with various tree distributions at nadir, while errors appear at off-nadir angles for forest stands with tree distributions deviating from the Poisson model, especially for forest plantations with obvious orientation or azimuth effects and forests on slope terrains. Only canopy and crown closures at nadir were used in the previous two Nilson's canopy GF models are insufficient to accurately calculate canopy GF at off-nadir. It makes canopy GFs identical for all forests with the same canopy closure at nadir. For example, the canopy closure in stand HG2, HG3, and HG4 in Figure 1, and LS1 and CS1 in Figure 2 is the same. The variations of canopy GF with zenith angle should be influenced by the zenith angular variation of crown projection area (see Eq. 11, 15) as well as OAC. We highly praise the ability of accurate expression of OAC at nadir for forests with various tree distributions in two Nilson's models and expanded this ability from nadir direction to other directions to accurately calculate canopy GF at off-nadir in the new models.

Tree distribution, often referring to the spatial arrangement or pattern of trees at nadir within a particular area (e.g., a forest stand) or ecosystem, is an essential parameter to calculate canopy GF

because it strongly influences the OAC and between-crown gaps. For example, tree distribution parameter is a constant in all directions and OAC is often simplified at off-nadir in many existing canopy BRF models. In this study, it might be more reasonable to stress that the tree distribution is related to certain directions because the signal (e.g., reflectance) obtained by remote sensors is inevitably influenced by directions, including view directions and sun directions. For instance, tree distribution in HET-14 in RAMI platform shows regularity at nadir (see Figure 10 (b)), while it shows clumping effect in Figure 10 (d). Although tree distribution has been widely studied in the field of ecology and forest inventory, it might be not enough for remote sensing because both nadir and off-nadir angles are concerned in the field of remote sensing, especially for multiple angular remote sensing. Tree distribution has been reported to strongly affect the forest coverage and canopy GF at nadir, yet the results in this study show it also strongly affects canopy GF at off-nadir. Essentially, they are just different projections on different planes or directions, i.e., from nadir to off-nadir. As both remote sensing and photogrammetry are based on projection, e.g., image, we prefer to use a directional tree distribution on VPP or image rather than tree distribution at nadir to calculate directional canopy GF accurately in these fields although the tree distribution often refers in particular to at nadir in ecology. Because the tree distribution at nadir is insufficient to describe the directional OAC and to calculate directional canopy GF as shown in section Results.

6.2 Limitations and applicability

The outcomes in this study show that the presented models (especially for New99) produce obviously better canopy GF simulations than the previous two Nilson's models for all forest stands, especially for forest stands with tree distributions deviating from the Poisson model. The tree distribution parameters $c_B(\theta)$ and $c(\theta)$ are derived from Fisher's group index GI in Eq. 20 and 21,

respectively. The difference between New91 and New99 exists in the position of the item (1- $p_c(\theta)$) in Eq. 18 and 21. Although both two new models show better consistency with the RT results than the two Nilson's models, New99 results generally show higher consistency with ray-tracing results than New91 in many cases. Therefore, New99 is more universal and accurate than New91. Except for some extreme cases, the differences between New99 and New91 are generally not obvious as shown in section Results.

The complicated scenarios of forests with various tree distributions, orientation or azimuth effects at different spatial scales on horizontal and sloping terrains are built to show the generality of the new models. The essence of two Nilson's models and two new models is the accurate calculation of OAC, which is strongly affect canopy GF. Crown GF (i.e., p_c in Eq. 5, 11, 16, 18, and 19) is another factor influencing the calculation of canopy GF. There is a common assumption in these models that leaves within an individual crown are randomly distributed. This assumption has been widely made in many forest canopy BRF models, e.g., FRT (Kuusk et al., 2014), GOMS (Wu et al., 2019b), a 4-scale geometric optical model for broad-leaved forests (Chen and Leblanc, 1997), GOST (Fan et al., 2015; Fan Weiliang et al., 2014), and GOFP (Geng et al., 2022a, 2017). For forests with non-notable sub-crown structures, it is not easy to measure the sub-crown structures and describe the complicated structure within crown with mathematical expressions, especially for broad-leaved forests. The sub-crown structures were expressed in the literature and were suggested to be considered for forests with notable sub-crown structures (Geng et al., 2016b; Leblanc et al., 1999), e.g., crown GF calculations considering notable shoot structure for conifer forests in a four scale geometric optical model (Chen and Leblanc, 1997), branch structures in a five-scale geometric optical model (Leblanc et al., 1999; Leblanc and Chen, 2000), and whorl structures in GORT (Wenge Ni et al., 1999). In this

case, crown GF is suggested to be calculated first by more accurate expressions in above literature instead of Eq. 5 in this study. After accurate calculation of crown GF for these forests, canopy GF can be calculated with the new models in this study.

Generally, a forest canopy model should only be applicable to a forest stand that is large enough to possess certain statistical properties, and not mean to be used for individual trees or a small patch of trees. For instance, a forest stand is divided into several quadrats, and counting the tree number in each quadrat is a common measurement of tree distribution *in situ*. Then, the probability density function or the expectation and variance are plotted and calculated, respectively (Chen and Leblanc, 1997; Penttinen and Stoyan, 2000; Perry et al., 2006; Diggle, 2013; Geng et al., 2021). Thus, the stand area or the spatial scale cannot be too small (e.g., often larger than 50 m), and the quadrat area is often larger than 10 m to ensure the statistic meaning. This problem also exists in the Nilson's models and the new models in this study. While available spatial scale in the Nilson's models and the two new models could be smaller than the Neyman type-A model. Theoretically, two Nilson's models and the two new models are suitable for a forest canopy with only one crown because the quadrat used for counting tree number in parameter GI is the projected area of a single crown according to the definition of GI (Nilson and Peterson, 1991; Nilson, 1999). GF of canopy with only one crown can be calculated as follows,

$$P(\theta) = (1 - C'_{CR}(\theta)) \cdot 1 + C'_{CR}(\theta) \cdot p_c(\theta) \tag{25}$$

Canopy GF in Eq. 25 is equal to that in Eq. 18 (New99). Yet, the crown projected area might be out of stand bound leading to a serious boundary problem if stand area is too small. A forest canopy needs to be a stand with enough large area, otherwise it can not be deemed as a canopy, e.g., a pixel in image with high spatial resolution (less than 1 m) may be deemed as a crown or sub-crown rather than a

canopy. A forest canopy GF model itself is a model simulated GF for a canopy rather than a crown or sub-crown.

6.3 Parameter Measurements

As reported in (Nilson, 1999; Nilson and Peterson, 1991), a simple handheld device (e.g., a digital hemispherical photography) consisting of a fine tube fixed on a cardan joint and a mirror below the tube helps the observer to look vertically upwards through the tube and thus carry out a point-wise sampling. Crown closure C_{CR} can be measured by the average number of overlaps, and canopy closure C_{CAN} is calculated as one minus the zero overlap probability. The tree distribution parameter GI is calculated by those two critical input parameters C_{CR} and C_{CAN}. Similar approach can be adopted from nadir to off-nadir. Digital hemispherical photos from down to up are well available, and the Cajanus tube can be replaced for off-nadir measurements now. The input parameters in the new models are similar to the previous Nilson's models, and the measurements of the tree distribution or OAC in a forest stand at nadir can be expanded to at off-nadir. If the structures of tree in a forest stand are similar (e.g., a forest plantations stand), $C_{CR}(0)$ can be directly estimated by Eq. 13, and $C_{CR}(\theta)$ can be calculated according to Eq. 23.

Image classification from up to down provide another method to calculate directional C_{CR} and C_{CAN} in the field as shown in section Validation. Recently, the airborne LiDAR (ALS) or terrestrial laser scanning (TLS) are proven capable of measuring the accurate directional crown and canopy closures. It has been reported that the individual crown segmentation could be completed well by those new techniques (Li et al., 2023; Chehreh et al., 2023; Pang et al., 2021; Zhang et al., 2020; Ayrey et al., 2017; Zhen et al., 2016; Chen et al., 2006). Directional C_{CR} can be easily calculated by summing all directional individual crown projected area divided by the ground projected area. The directional

between-crown gaps can be easily calculated in the virtual forests scene with amount of point cloud, and directional C_{CAN} can be calculated by 1 minus the directional between-crown gaps as shown in section Validation.

6.4 Meaning of a universal canopy GF model and future studies

As canopy GF is a fundamental and a critical parameter that influences many other parameters, e.g., bi-directional canopy GF, clumping index, reflectance or bidirectional reflectance factor (known as BRF), emissivity, and LAI, etc, the new models in this study are full of meaning.

(1) A potential tool for a universal canopy BRF model for forests with various tree distributions on horizontal and sloping terrains at multiple spatial scales

Canopy GF is often the first step to be calculated in canopy BRF models. The existing geometric optical and radiative transfer models are reported to be suitable for certain cases because the tree distribution is described for these cases. For example, a four-scale and a five-scale geometric optical models were developed for forests with clumped tree distributions at large scales (often lager than 250 m) because the Neyman type-A model was used to describe tree distributions and calculate canopy GF (Chen and Leblanc, 1997; Leblanc and Chen, 2000); GOFP was reported to be suitable for regular tree distributions at small scales (often less than 100 m) because of the hypergeometric canopy GF model was used (Geng et al., 2021). Based on the previous Nilson's canopy GF models, FRT and ACRM show more adaptive (Kuusk, 1995, 2001; Kuusk et al., 2014), while they are also hard to accurately simulate reflectance for forest plantations at off-nadir (e.g., stands in Figure 2) because the previous Nilson's canopy GF models were used in these models (e.g., canopy GF in Figure 5). In addition, all above-mentioned BRF models do not consider the forest stand orientation or azimuth effect. The universal canopy GF models presented in this study makes a universal BRF model possible.

(2) A new opinion to the variation of canopy GF and clumping index with zenith angle

As canopy GF is closely related to crown GF and OAC as mentioned above. It means that the variation of canopy GF with zenith angle is closely related to directional crown GF and OAC as shown in section Results. Foliage clumping index is defined as a ratio of the effective LAI (LAI_e) to LAI (Chen et al., 2005; Fang, 2021; Nilson, 1971). LAI_e is the LAI value that would produce the same indirect gap measurement (e.g., canopy GF) as that observed, assuming a simple random foliage distribution and it is often measured by many optical instruments (e.g., LAI-2000 and digital hemispherical photography) based on the theory of Beer-Lambert's theory (Fang, 2021). Therefore, foliage clumping index is closely related to canopy GF.

It is widely accepted that clumping index is often related to zenith angle, i.e., clumping index might be varied with zenith angle. The variations of clumping index with zenith angle in *situ* measurements show different results in the literature (Fang et al., 2018b, 2018a; Geng et al., 2022b; Kucharik et al., 1999). Recently, it was reported that the crown size or the angular variation of crown projection area is of critical influence on zenith angular variations of clumping index for forests. The results were based on the theoretical derivations derived from the previous Nilson's canopy GF model (Nilson99) which clearly considered the OAC at nadir but simplified at off-nadir. For the two Nilson's models, the variation of canopy GF with zenith angle is mainly affected by the variation of crown projection with zenith angle (Nilson, 1999). The results in this study show the zenith angular variation of clumping index must be closely related to both crown projection area and OAC. Therefore, a new study about the zenith angular variations of clumping index for forests is advised.

(3) A potential tool for better understanding of the spatial scale effect of parameter retrievals with satellite image

Spatial scale effect is a topic in the filed of remote sensing. The heterogeneity of forest canopy is an essential reason for spatial scale effect of parameter retrievals with remote sensing image with different spatial resolutions. It is reported that trees often show different distribution patterns at different spatial scales, which plays a critical role in the heterogeneity of the forest canopy and the spatial scale effect of parameter retrievals at multiple spatial scales (Chen and Leblanc, 1997; Liang, 2000; Li et al., 2000; Jin et al., 2007; Zhan et al., 2012; Jiang, 2018; Geng et al., 2021).

The scale problem of canopy GF can hardly be analyzed by the previous forests canopy GF models because there is a lack of a universal canopy GF model suitable for forests at multiple spatial scales (e.g., from 30 m to 1 km). The two universal canopy GF models presented in this study provide a potential tool to process this problem. They are well designed for studying the spatial scale effect of signal forward simulations and parameters retrieval with remote sensing technique because they can be applied at multiple spatial scales. The new models provide an important link in canopy GF and other relative parameters (e.g., fAPAR, clumping index and LAI_e) among different spatial scales and useful tools for better understanding down-scaling and up-scaling studies and applications of satellite remote sensing between medium and low spatial resolutions, e.g., MODIS and Landsat OLI.

7 Conclusions

A forest canopy GF model suitable for different types of tree distributions is critical for forest canopy reflectance modelling because canopy GF is the basis for canopy reflectance modeling and parameter retrievals based on remote sensing techniques. As there is still a lack of In this study,

(1) we found the overlap among crowns (OAC) at off-nadir was simplified in two Nilson's models, expanded the calculation of OAC at nadir in two Nilson's models to other directions, and finally developed two new canopy GF models (New99 and New91) based on the Nilson99 and Nilson91,

respectively.

(2) the canopy GF simulations by the two new models (especially for New99) show high consistency with the ray-tracing results in forests with various tree distribution patterns at different zenith angles and spatial scales on horizontal and sloping terrains. While the original Nilson's models underestimate canopy GF for forests with clumped tree distributions or overestimate canopy GF for regular tree distributions at off-nadir, which could be amplified in the cases of forest plantations and forest stands on sloping terrains. New99 effectively improves the accuracy of canopy GF simulations in all those forests, showing its universality in simulating canopy GF for forests. It could form the backbone of the development of a potentially universal canopy reflectance model since a cutting-edge modeling of the transmittance of the photons pathway is primarily meaningful for forest stands.

Acknowledgement

This study was mainly supported by National Natural Science Foundation of China, grant number 41701383 and 41801234; Anhui Provincial Natural Science Foundation, grant number 2208085MD90; the Fundamental Research Funds for the Central Universities, grant number JZ2022HGTB0253; the funding from the China Scholarship Council scholarship (No. 202006695009). Andres Kuusk was supported by the Estonian Research Council grant PRG1405.

References

Atzberger, C., 2000. Development of an invertible forest reflectance model: The INFOR-Model. In M. Buchroithner (Ed.), A decade of Trans-European remote sensing cooperation. Proceedings of the 20th EARSeL Symposium Dresden, Germany, 14–16 June 2000 (pp. 39–44). Leiden, The Netherlands:

CRC Press/Balkema.

Ayrey, E., Fraver, S., Kershaw, J.A., Kenefic, L.S., Hayes, D., Weiskittel, A.R., Roth, B.E., 2017. Layer Stacking: A Novel Algorithm for Individual Forest Tree Segmentation from LiDAR Point Clouds. Canadian Journal of Remote Sensing 43, 16–27. https://doi.org/10.1080/07038992.2017.1252907

Chehreh, B., Moutinho, A., Viegas, C., 2023. Latest Trends on Tree Classification and Segmentation Using UAV Data—A Review of Agroforestry Applications. Remote Sensing 15, 2263. https://doi.org/10.3390/rs15092263

Chen, J.M., Black, T.A., 1992. Defining leaf area index for non-flat leaves. Plant Cell Environ 15, 421–429. https://doi.org/10.1111/j.1365-3040.1992.tb00992.x

Chen, J.M., Leblanc, S.G., 1997. A Four-Scale Bidirectional Reflectance Model Based on Canopy Architecture. IEEE TRANSACTIONS ON GEOSCIENCE AND REMOTE SENSING 35, 1316–1337. https://doi.org/10.1109/36.628798

Chen, J.M., Menges, C.H., Leblanc, S.G., 2005. Global mapping of foliage clumping index using multi-angular satellite data. Remote Sensing of Environment 97, 447–457. https://doi.org/10.1016/j.rse.2005.05.003

Chen, Q., Baldocchi, D., Gong, P., Kelly, M., 2006. Isolating Individual Trees in a Savanna Woodland Using Small Footprint Lidar Data. Photogrammetric Engineering & Remote Sensing 72, 923–932. https://doi.org/10.14358/PERS.72.8.923

Diggle, P.J., 2013. Statistical analysis of spatial and spatio-temporal point patterns. CRC press.

Fan, W., Li, J., Liu, Q., 2015. GOST2: The Improvement of the Canopy Reflectance Model GOST in Separating the Sunlit and Shaded Leaves. IEEE J. Sel. Top. Appl. Earth Observations Remote Sensing

8, 1423–1431. https://doi.org/10.1109/JSTARS.2015.2413994

Fan Weiliang, Chen, J.M., Weimin Ju, Gaolong Zhu, 2014. GOST: A Geometric-Optical Model for Sloping Terrains. IEEE Trans. Geosci. Remote Sensing 52, 5469–5482. https://doi.org/10.1109/TGRS.2013.2289852

Fang, H., 2021. Canopy clumping index (CI): A review of methods, characteristics, and applications. Agricultural and Forest Meteorology 303, 108374. https://doi.org/10.1016/j.agrformet.2021.108374

Fang, H., Liu, W., Li, W., Wei, S., 2018a. Estimation of the directional and whole apparent clumping index (ACI) from indirect optical measurements. ISPRS Journal of Photogrammetry and Remote Sensing 144, 1–13. https://doi.org/10.1016/j.isprsjprs.2018.06.022

Fang, H., Ye, Y., Liu, W., Wei, S., Ma, L., 2018b. Continuous estimation of canopy leaf area index (LAI) and clumping index over broadleaf crop fields: An investigation of the PASTIS-57 instrument and smartphone applications. Agricultural and Forest Meteorology 253–254, 48–61. https://doi.org/10.1016/j.agrformet.2018.02.003

Geng, J., Chen, J.M., Fan, W., Tu, L., Pang, Y., Yuan, G., Xu, L., Zhu, C., Zhang, T., Zhang, C., Ye, Z., Zhu, Y., Li, Z., 2022a. Application of a Hypergeometric Model in Simulating Canopy Gap Fraction and BRF for Forest Plantations on Sloping Terrains. IEEE J. Sel. Top. Appl. Earth Observations Remote Sensing 15, 2901–2913. https://doi.org/10.1109/JSTARS.2022.3156403

Geng, J., Chen, J.M., Fan, W., Tu, L., Tian, Q., Yang, R., Yang, Y., Wang, L., Lv, C., Wu, S., 2017. GOFP: A Geometric-Optical Model for Forest Plantations. IEEE Trans. Geosci. Remote Sensing 55, 5230–5241. https://doi.org/10.1109/TGRS.2017.2704079

Geng, J., Chen, J.-M., Tu, L.-L., Tian, Q.-J., Wang, L., Yang, R.-R., Yang, Y.-J., Huang, Y., Fan, W.-L., Lv, C.-G., Zheng, G., 2016a. Influence of the exclusion distance among trees on gap fraction

and foliage clumping index of forest plantations. Trees 30, 1683–1693. https://doi.org/10.1007/s00468-016-1400-y

Geng, J., Tu, L., Chen, J.M., Roujean, J.-L., Yuan, G., Hu, R., Huang, J., Zhang, C., Ye, Z., Qu, X., Yu, M., Zhu, Y., Tian, Q., 2022b. Variation of Clumping Index With Zenith Angle for Forest Canopies. IEEE Trans. Geosci. Remote Sensing 60, 1–11. https://doi.org/10.1109/TGRS.2022.3226154

Geng, J., Tu, L., Tian, Q., Wang, X., Zhu, X., Yang, Y., Yang, R., Wang, L., Lv, C., Fang, Y., 2016b. Influence of branch architectures on gap fraction and clumping index of canopies, in: 2016 IEEE International Geoscience and Remote Sensing Symposium (IGARSS). Presented at the IGARSS 2016 - 2016 IEEE International Geoscience and Remote Sensing Symposium, IEEE, Beijing, China, pp. 1311–1314. https://doi.org/10.1109/IGARSS.2016.7729333

Geng, J., Zhang, Q., Qiu, F., Chen, J.M., Zhang, Y., Fan, W., Tu, L., Huang, J., Wang, S., Xu, L., Li, J., 2021. Evaluation of GOFP over four forest plots using RAMI and UAV measurements. International Journal of Digital Earth 14, 1433–1451. https://doi.org/10.1080/17538947.2021.1936226

Goel, N.S., Thompson, R.L., 2000. A snapshot of canopy reflectance models and a universal model for the radiation regime. Remote Sensing Reviews 18, 197–225. https://doi.org/10.1080/02757250009532390

Gonsamo, A., Walter, J.-M.N., Pellikka, P., 2011. CIMES: A package of programs for determining canopy geometry and solar radiation regimes through hemispherical photographs. Computers and Electronics in Agriculture 79, 207–215. https://doi.org/10.1016/j.compag.2011.10.001

Illian, J., Penttinen, A., Stoyan, H., Stoyan, D., 2007. Statistical Analysis and Modelling of Spatial Point Patterns, 1st ed. Wiley. https://doi.org/10.1002/9780470725160

Jiang, B., 2018. Spatial Heterogeneity, Scale, Data Character and Sustainable Transport in the Big Data

Era. IJGI 7, 167. https://doi.org/10.3390/ijgi7050167

Jiao, Z., Dong, Y., Schaaf, C.B., Chen, J.M., Román, M., Wang, Z., Zhang, H., Ding, A., Erb, A., Hill, M.J., Zhang, X., Strahler, A., 2018. An algorithm for the retrieval of the clumping index (CI) from the MODIS BRDF product using an adjusted version of the kernel-driven BRDF model. Remote Sensing of Environment 209, 594–611. https://doi.org/10.1016/j.rse.2018.02.041

Jin, Z., Tian, Q., Chen, J.M., Chen, M., 2007. Spatial scaling between leaf area index maps of different resolutions. Journal of Environmental Management 85, 628–637. https://doi.org/10.1016/j.jenvman.2006.08.016

Jonckheere, I., Fleck, S., Nackaerts, K., Muys, B., Coppin, P., Weiss, M., Baret, F., 2004. Review of methods for in situ leaf area index determination. Agricultural and Forest Meteorology 121, 19–35. https://doi.org/10.1016/j.agrformet.2003.08.027

Knyazikhin, Y., Martonchik, J.V., Myneni, R.B., Diner, D.J., Running, S.W., 1998. Synergistic algorithm for estimating vegetation canopy leaf area index and fraction of absorbed photosynthetically active radiation from MODIS and MISR data. J. Geophys. Res. 103, 32257–32275. https://doi.org/10.1029/98JD02462

Kucharik, C.J., Norman, J.M., Gower, S.T., 1999. Characterization of radiation regimes in nonrandom forest canopies: theory, measurements, and a simplified modeling approach. Tree Physiology 19, 695–706. https://doi.org/10.1093/treephys/19.11.695

Kuusk, A., 2018. Canopy Radiative Transfer Modeling, in: Comprehensive Remote Sensing. Elsevier, pp. 9–22. https://doi.org/10.1016/B978-0-12-409548-9.10534-2

Kuusk, A., 2001. A two-layer canopy reflectance model. Journal of Quantitative Spectroscopy and Radiative Transfer 71, 1–9. https://doi.org/10.1016/S0022-4073(01)00007-3

Kuusk, A., 1995. A fast, invertible canopy reflectance model. Remote Sensing of Environment 51, 342–350. https://doi.org/10.1016/0034-4257(94)00059-V

Kuusk, A., Kuusk, J., Lang, M., 2014. Modeling directional forest reflectance with the hybrid type forest reflectance model FRT. Remote Sensing of Environment 149, 196–204. https://doi.org/10.1016/j.rse.2014.03.035

Kuusk, A., Nilson, T., 2000. A Directional Multispectral Forest Reflectance Model. Remote Sensing of Environment 72, 244–252. https://doi.org/10.1016/S0034-4257(99)00111-X

Lang, M., Kuusk, A., Vennik, K., Liibusk, A., Türk, K., Sims, A., 2021. Horizontal Visibility in Forests. Remote Sensing 13, 4455. https://doi.org/10.3390/rs13214455

Law, R., Illian, J., Burslem, D.F.R.P., Gratzer, G., Gunatilleke, C.V.S., Gunatilleke, I.A.U.N., 2009. Ecological information from spatial patterns of plants: insights from point process theory. Journal of Ecology 97, 616–628. https://doi.org/10.1111/j.1365-2745.2009.01510.x

Leblanc, S.G., Bicheron, P., Chen, J.M., Leroy, M., Cihlar, J., 1999. Investigation of directional reflectance in boreal forests with an improved four-scale model and airborne POLDER data. IEEE Trans. Geosci. Remote Sensing 37, 1396–1414. https://doi.org/10.1109/36.763304

Leblanc, S.G., Chen, J.M., 2000. A windows graphic user interface (GUI) for the five-scale model for fast BRDF simulations. Remote Sensing Reviews 19, 293–305. https://doi.org/10.1080/02757250009532423

Li, X., Strahler, A., 1985. Geometric-Optical Modeling of a Conifer Forest Canopy. IEEE Trans. Geosci. Remote Sensing GE-23, 705–721. https://doi.org/10.1109/TGRS.1985.289389

Li, X., Wang, J., Strahler, A.H., 2000. Scale effects and scaling-up by geometric-optical model. Sci. China Ser. E-Technol. Sci. 43, 17–22. https://doi.org/10.1007/BF02916574

Li, Y., Xie, D., Wang, Y., Jin, S., Zhou, K., Zhang, Z., Li, W., Zhang, W., Mu, X., Yan, G., 2023. Individual tree segmentation of airborne and UAV LiDAR point clouds based on the watershed and optimized connection center evolution clustering. Ecology and Evolution 13, e10297. https://doi.org/10.1002/ece3.10297

Liang, S., 2000. Numerical experiments on the spatial scaling of land surface albedo and leaf area index. Remote Sensing Reviews 19, 225–242. https://doi.org/10.1080/02757250009532420

Myneni, R.B., Ramakrishna, R., Nemani, R., Running, S.W., 1997. Estimation of global leaf area index and absorbed par using radiative transfer models. IEEE Trans. Geosci. Remote Sensing 35, 1380–1393. https://doi.org/10.1109/36.649788

Nilson, T., 1999. Inversion of gap frequency data in forest stands. Agricultural and Forest Meteorology 98–99, 437–448. https://doi.org/10.1016/S0168-1923(99)00114-8

Nilson, T., 1971. A theoretical analysis of the frequency of gaps in plant stands. Agricultural Meteorology 8, 25–38. https://doi.org/10.1016/0002-1571(71)90092-6

Nilson, T., Peterson, U., 1991. A forest canopy reflectance model and a test case. Remote Sensing of Environment 37, 131–142. https://doi.org/10.1016/0034-4257(91)90024-Z

Pang, Y., Wang, W., Du, L., Zhang, Z., Wang, Z., 2021. Nystrm-based spectral clustering using airborne LiDAR point cloud data for individual tree segmentation. International Journal of Digital Earth 1–25. https://doi.org/10.1080/17538947.2021.1943018

Penttinen, A., Stoyan, D., 2000. Recent applications of point process methods in forestry statistics. Statist. Sci. 15. https://doi.org/10.1214/ss/1009212674

Perry, G.L.W., Miller, B.P., Enright, N.J., 2006. A comparison of methods for the statistical analysis of spatial point patterns in plant ecology. Plant Ecol 187, 59–82.

https://doi.org/10.1007/s11258-006-9133-4

Qi, J., Xie, D., Yin, T., Yan, G., Gastellu-Etchegorry, J.-P., Li, L., Zhang, W., Mu, X., Norford, L.K., 2019. LESS: LargE-Scale remote sensing data and image simulation framework over heterogeneous 3D scenes. Remote Sensing of Environment 221, 695–706. https://doi.org/10.1016/j.rse.2018.11.036

Rosema, A., Verhoef, W., Noorbergen, H., Borgesius, J.J., 1992. A new forest light interaction model in support of forest monitoring. Remote Sensing of Environment 42, 23–41. https://doi.org/10.1016/0034-4257(92)90065-R

Ross, J., 1981. The radiation regime and architecture of plant stands. W. Junk Publishers, The Hague. https://doi.org/10.1007/978-94-009-8647-3

Roujean, J.-L., 2002. Global mapping of vegetation parameters from POLDER multiangular measurements for studies of surface-atmosphere interactions: A pragmatic method and its validation. J. Geophys. Res. 107, 4150. https://doi.org/10.1029/2001JD000751

Weiss, M., Baret, F., Smith, G.J., Jonckheere, I., Coppin, P., 2004. Review of methods for in situ leaf area index (LAI) determination. Agricultural and Forest Meteorology 121, 37–53. https://doi.org/10.1016/j.agrformet.2003.08.001

Wenge Ni, Xiaowen Li, Woodcock, C.E., Caetano, M.R., Strahler, A.H., 1999. An analytical hybrid GORT model for bidirectional reflectance over discontinuous plant canopies. IEEE Trans. Geosci. Remote Sensing 37, 987–999. https://doi.org/10.1109/36.752217

Widlowski, J.-L., Mio, C., Disney, M., Adams, J., Andredakis, I., Atzberger, C., Brennan, J., Busetto, L., Chelle, M., Ceccherini, G., Colombo, R., Côté, J.-F., Eenmäe, A., Essery, R., Gastellu-Etchegorry, J.-P., Gobron, N., Grau, E., Haverd, V., Homolová, L., Huang, H., Hunt, L., Kobayashi, H., Koetz, B., Kuusk, A., Kuusk, J., Lang, M., Lewis, P.E., Lovell, J.L., Malenovský, Z., Meroni, M., Morsdorf, F.,

Mõttus, M., Ni-Meister, W., Pinty, B., Rautiainen, M., Schlerf, M., Somers, B., Stuckens, J., Verstraete, M.M., Yang, W., Zhao, F., Zenone, T., 2015. The fourth phase of the radiative transfer model intercomparison (RAMI) exercise: Actual canopy scenarios and conformity testing. Remote Sensing of Environment 169, 418–437. https://doi.org/10.1016/j.rse.2015.08.016

Wu, S., Wen, J., Lin, X., Hao, D., You, D., Xiao, Q., Liu, Q., Yin, T., 2019a. Modeling Discrete Forest Anisotropic Reflectance Over a Sloped Surface With an Extended GOMS and SAIL Model. IEEE Trans. Geosci. Remote Sensing 57, 944–957. https://doi.org/10.1109/TGRS.2018.2863605

Wu, S., Wen, J., Lin, X., Hao, D., You, D., Xiao, Q., Liu, Q., Yin, T., 2019b. Modeling Discrete Forest Anisotropic Reflectance Over a Sloped Surface With an Extended GOMS and SAIL Model. IEEE Trans. Geosci. Remote Sensing 57, 944–957. https://doi.org/10.1109/TGRS.2018.2863605

Yin, G., Ma, L., Zhao, W., Zeng, Y., Xu, B., Wu, S., 2020. Topographic Correction for Landsat 8 OLI Vegetation Reflectances Through Path Length Correction: A Comparison Between Explicit and Implicit Methods. IEEE Trans. Geosci. Remote Sensing 58, 8477–8489. https://doi.org/10.1109/TGRS.2020.2987985

Zhan, W., Chen, Y., Wang, J., Zhou, J., Quan, J., Liu, W., Li, J., 2012. Downscaling land surface temperatures with multi-spectral and multi-resolution images. International Journal of Applied Earth Observation and Geoinformation 18, 23–36. https://doi.org/10.1016/j.jag.2012.01.003

Zhang, W., Cai, S., Liang, X., Shao, J., Hu, R., Yu, S., Yan, G., 2020. Cloth simulation-based construction of pit-free canopy height models from airborne LiDAR data. Forest Ecosystems 7, 1. https://doi.org/10.1186/s40663-019-0212-0

Zhen, Z., Quackenbush, L.J., Zhang, L., 2016. Trends in Automatic Individual Tree Crown Detection and Delineation—Evolution of LiDAR Data. Remote Sensing 8, 333.

https://doi.org/10.3390/rs8040333